

# Weak Gravitational Lensing

S. Pires, J.-L. Starck, A. Leonard and A. Réfrégier  
Laboratoire AIM, CEA/DSM-CNRS-Universite Paris Diderot,  
IRFU/SEDI-SAP, CEA Saclay,  
Orme des Merisiers, 91191 Gif-sur-Yvette, France

August 4, 2011

## Contents

<b>1</b>	<b>Introduction</b>	<b>2</b>
<b>2</b>	<b>Weak Lensing theory</b>	<b>4</b>
<b>3</b>	<b>Shear estimation</b>	<b>8</b>
3.1	Basics . . . . .	9
3.2	Biases . . . . .	10
3.3	Challenges . . . . .	13
<b>4</b>	<b>2D mapping of the dark matter</b>	<b>14</b>
4.1	Inversion problem . . . . .	14
4.2	E and B modes decomposition . . . . .	15
4.3	Missing data . . . . .	16
4.4	Filtering . . . . .	18
<b>5</b>	<b>3D mapping of the dark matter</b>	<b>21</b>
5.1	Formalism . . . . .	22
5.2	Filtering . . . . .	23
<b>6</b>	<b>Cosmological model constraints</b>	<b>25</b>
6.1	Methodology . . . . .	25
6.2	Second-order statistics . . . . .	26
6.3	Non-Gaussian statistics . . . . .	29
<b>7</b>	<b>Conclusion</b>	<b>32</b>

# 1 Introduction

This chapter reviews the data mining methods recently developed to solve standard data problems in weak gravitational lensing. We detail the different steps of the weak lensing data analysis along with the different techniques dedicated to these applications. An overview of the different techniques currently used will be given along with future prospects.

Until about thirty years ago astronomers thought that the Universe was composed almost entirely of ordinary matter: protons, neutrons, electrons and atoms. The field of weak lensing has been motivated by the observations made in the last decades showing that visible matter represents only about 4-5% of the Universe (see Fig. 1). Currently, the majority of the Universe is thought to be dark, i.e. does not emit electromagnetic radiation. The Universe is thought to be mostly composed of an invisible, pressureless matter - potentially relic from higher energy theories - called “dark matter” (20-21%) and by an even more mysterious term, described in Einstein equations as a vacuum energy density, called “dark energy” (70%). This “dark” Universe is not well described or even understood; its presence is inferred indirectly from its gravitational effects, both on the motions of astronomical objects and on light propagation. So this point could be the next breakthrough in cosmology.

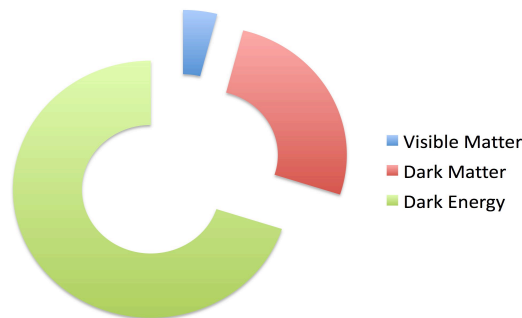


Figure 1: Universe content

Today’s cosmology is based on a cosmological model that contains various parameters that need to be determined precisely, such as the matter density parameter  $\Omega_m$  or the dark energy density parameter  $\Omega_\Lambda$ . Weak gravitational lensing is believed to be the most promising tool to understand the nature of dark matter and to constrain the cosmological parameters used to describe the Universe because it provides a method to map directly the distribution of dark matter (see [6, 61, 70, 1, 64]). From this dark matter distribution, the nature of dark matter can be better understood and better constraints can be placed on dark energy, which affects the evolution of structures. Gravitational lensing is the process by which light from distant galaxies is bent by the gravity of intervening mass in the Universe as it travels towards us. This bending causes

the images of background galaxies to appear slightly distorted, and can be used to extract important cosmological information.

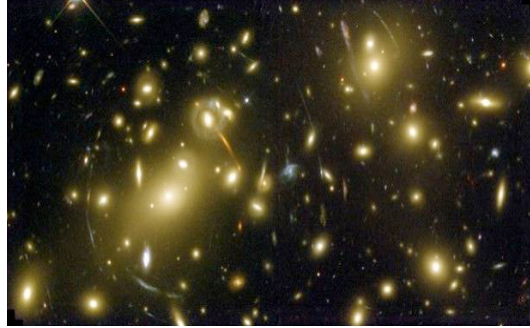


Figure 2: Strong Gravitational Lensing effect observed in the Abell 2218 cluster (W. Couch et al, 1975 - HST). Photo used with permission from NASA, ESA and the ERO team.

In the beginning of the twentieth century, A. Einstein predicted that massive bodies could be seen as gravitational lenses that bend the path of light rays by creating a local curvature in space-time. One of the first confirmations of Einstein's new theory was the observation during the 1919 solar eclipse of the deflection of light from distant stars by the sun. Since then, a wide range of lensing phenomena have been detected. The gravitational deflection of light by mass concentrations along light paths produces magnification, multiplication, and distortion of images. These lensing effects are illustrated by Fig. 2, which shows one of the strongest lens observed: Abell 2218, a very massive and distant cluster of galaxies in the constellation Draco. The observed gravitational arcs are actually the magnified and strongly distorted images of galaxies that are about 10 times more distant than the cluster itself.

These strong gravitational lensing effects are very impressive but they are very rare. Far more prevalent are weak gravitational lensing effects, which we consider in this chapter, and in which the induced distortion in galaxy images is much weaker. These gravitational lensing effects are now widely used, but the amplitude of the weak lensing signal is so weak that its detection relies on the accuracy of the techniques used to analyze the data. Future weak lensing surveys are already planned in order to cover a large fraction of the sky with high accuracy, such as Euclid. However improving accuracy also places greater demands on the methods used to extract the available information.

## 2 Weak Lensing theory

A gravitational lens is formed when the light from a very distant galaxy is deflected around a massive object between the source and the observer. The properties of the gravitational lensing effect depend on the projected mass den-

sity integrated along the line of sight and on the cosmological angular distances between the observer, the lens and the source (see Fig. 3). The bending of light rays around massive objects makes the images of distant galaxies appear deformed. The gravitational lensing causes a tangential alignment of the source. From the measurement of these distortions, the distribution of the intervening mass can be inferred.

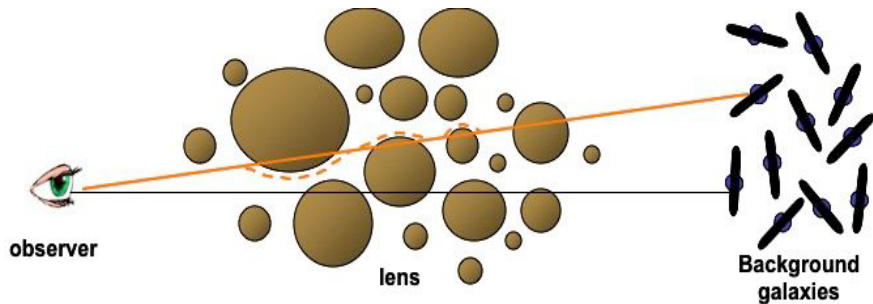


Figure 3: Illustration of the gravitational lensing effect by large scale structures: the light coming from distant galaxies (on the right) traveling toward the observer (on the left) is bent by the structures (in the middle). This bending causes the image of background galaxies to appear slightly distorted. The structures causing the deformations are called gravitational lenses by analogy with classical optics.

### The deflection angle

Light rays propagate along null geodesics, which correspond to the shortest path between two points in a curved spacetime. Therefore, to exactly compute the deflection of light rays around a massive object, it is necessary to determine the geometry of the Universe around that object by solving General-Relativistic equations. However, the problem can be simplified by making use of Fermat's principle, which states that light rays propagate along the path that minimises the light travel time between two points. Even though, according to the formalism of General Relativity, the path followed by light rays is an intrinsic property of space-time, while the travel time is an observer-dependent notion, the motion of light rays in a curved space time can still be described by this principle. A possible interpretation is to consider that light slows down in a gravitational field. The refractive index  $n$  in a gravitational field  $\Phi$  is given by:

$$n = 1 + \frac{2}{c^2}|\Phi| \quad (1)$$

where  $c$  is the speed of light and  $\Phi$  the 3D Newtonian potential, supposed to be weak ( $\Phi \ll c^2$ ).

Although the light speed in a vacuum is a constant  $c$  in General Relativity,

we assume that the speed of light in this disturbed region becomes:

$$c' = \frac{c}{n} = \frac{c}{1 + \frac{2}{c^2}|\Phi|} \quad (2)$$

Then, the light ray is bent and the deflection angle  $\alpha$  can be obtained by integrating the (perpendicular component of the) refractive index along the light path:

$$\vec{\alpha}(\vec{\xi}) = - \int \nabla_{\perp} n(\vec{r}) dz \quad (3)$$

where  $\vec{\xi}$  is the impact parameter in the lens plane (see Fig. 4) and  $\nabla_{\perp}$  is the perpendicular component of the gradient operator.

### The lens equation

In theory, light rays are bent by all the matter encountered along the light path between the source and the observer. Given that mass concentrations tend to be localised within the Universe, we may use the so-called thin lens approximation to simplify the problem. In this approximation, the lensing effect is supposed to come from a single matter inhomogeneity located on a plane between the source and the observer. This approximation is valid as long as the physical extent of the mass concentration is small compared to the lens-source, lens-observer and source-observer distances. The system is then divided into three planes: the source plane, the lens plane and the observer plane. The light ray is assumed to travel without deflection between these planes with just a slight deflection  $\alpha$  while crossing the lens plane (see Fig. 4). In the limit of a thin lens, all the physics of the gravitational lensing effect is contained in the lens equation, which relates the true position of the source  $\theta_S$  to its observed position(s) on the sky  $\theta_I$ :

$$\vec{\theta}_S = \vec{\theta}_I - \frac{D_{LS}}{D_{OS}} \vec{\alpha}(\vec{\xi}), \quad (4)$$

where  $\vec{\xi} = D_{OL}\vec{\theta}_I$  and  $D_{OL}$ ,  $D_{LS}$  and  $D_{OS}$  are the distance from the observer to the lens, the lens to the source, and the observer to the source, respectively. From equation 3, the deflection angle  $\alpha$  is related to the projected gravitational potential  $\phi$  obtained by the integration of the 3D Newtonian potential  $\Phi(\vec{r})$  along the line of sight:

$$\vec{\alpha}(\vec{\xi}) = \frac{2}{c^2} \int \nabla_{\perp} \Phi(\vec{r}) dz = \nabla_{\perp} \underbrace{\left( \frac{2}{c^2} \int \Phi(\vec{r}) dz \right)}_{\phi}. \quad (5)$$

We can distinguish two regimes of gravitational lensing. In most cases, the bending of light is small and the background galaxies are just slightly distorted. This corresponds to the weak lensing effect. Occasionally (as seen previously)

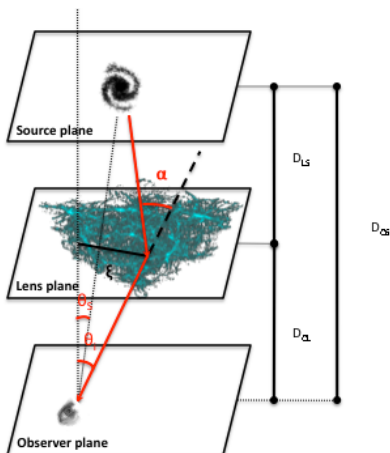


Figure 4: The thin lens approximation.

the bending of light is so extreme that the light travels along several different paths to the observer, and multiple images of one single source appear on the sky. Such effects are collectively termed strong lensing, and are typically seen where the angular position of the source is closely aligned with that of the centre of the mass concentration. In this chapter, we address only the weak gravitational lensing regime, in which sources are singly imaged and weakly distorted.

#### The distortion matrix $A$

The weak gravitational lensing effect results in both an isotropic dilation (the convergence,  $\kappa$ ) and an anisotropic distortion (the shear,  $\gamma$ ) of the source. To quantify this effect, the lens equation has to be solved. Assuming  $\theta_I$  is small, we may approximate the lens equation by a first order Taylor series expansion:

$$\theta_{S,i} = A_{ij}\theta_{I,j}, \quad (6)$$

where

$$A_{i,j} = \frac{\partial\theta_{S,i}}{\partial\theta_{I,j}} = \delta_{i,j} - \frac{\partial\alpha_i(\theta_{I,i})}{\partial\theta_{I,j}} = \delta_{i,j} - \frac{\partial^2\phi(\theta_{I,i})}{\partial\theta_{I,i}\partial\theta_{I,j}}, \quad (7)$$

$A_{i,j}$  are the elements of the matrix  $A$  and  $\delta_{i,j}$  is the Kronecker delta. The first order lensing effects (the convergence  $\kappa$  and the shear  $\gamma$ ) can be described by the Jacobian matrix  $A$ , called the distortion matrix:

$$A = (1 - \kappa) \begin{pmatrix} 1 & 0 \\ 0 & 1 \end{pmatrix} - \gamma \begin{pmatrix} \cos 2\varphi & \sin 2\varphi \\ \sin 2\varphi & -\cos 2\varphi \end{pmatrix}, \quad (8)$$

where  $\gamma_1 = \gamma \cos 2\varphi$  and  $\gamma_2 = \gamma \sin 2\varphi$  are the two components of the gravitational shear  $\gamma$ .

The convergence term  $\kappa$  magnifies the images of background objects, and the shear term  $\gamma$  stretches them tangentially around the foreground mass.

### The gravitational shear $\gamma$

The gravitational shear  $\gamma$  describes the anisotropic distortions of background galaxy images. It corresponds to a two component field,  $\gamma_1$  and  $\gamma_2$ , that can be derived from the shape of observed galaxies:  $\gamma_1$  describes the shear in the  $x$  and  $y$  directions and  $\gamma_2$  describes the shear in the  $x = y$  and  $x = -y$  directions. Using the lens equation, the two shear components  $\gamma_1$  and  $\gamma_2$  can be related to the gravitational potential  $\phi$  by:

$$\begin{aligned}\gamma_1 &= \frac{1}{2} \left[ \frac{\partial^2 \phi(\vec{\theta}_I)}{\partial \theta_{I,1}^2} - \frac{\partial^2 \phi(\vec{\theta}_I)}{\partial \theta_{I,2}^2} \right] \\ \gamma_2 &= \frac{\partial^2 \phi(\vec{\theta}_I)}{\partial \theta_{I,1} \partial \theta_{I,2}}.\end{aligned}\tag{9}$$

If a galaxy is initially circular with a diameter equal to 1, the gravitational shear will transform the galaxy image to an ellipsoid with a major axis  $a = \frac{1}{1-\kappa-|\gamma|}$  and a minor axis  $b = \frac{1}{1-\kappa+|\gamma|}$ . The eigenvalues of the amplification matrix (corresponding to the inverse of the distortion matrix  $A$ ) provide the elongation and the orientation produced on the images of lensed sources [61]. The shear  $\gamma$  is frequently represented by a line segment representing the amplitude and the direction of the distortion (see Fig. 5).

### The convergence $\kappa$

The convergence  $\kappa$ , corresponding to the isotropic distortion of background galaxy images, is related to the trace of the distortion matrix  $A$  by:

$$\begin{aligned}tr(A) &= \delta_{1,1} + \delta_{2,2} - \frac{\partial^2 \phi(\vec{\theta}_I)}{\partial \theta_{I,1}^2} - \frac{\partial^2 \phi(\vec{\theta}_I)}{\partial \theta_{I,2}^2}, \\ tr(A) &= 2 - \Delta \phi(\vec{\theta}_I) = 2(1 - \kappa).\end{aligned}\tag{10}$$

$$\kappa = \frac{1}{2} \left( \frac{\partial^2 \phi(\vec{\theta}_I)}{\partial \theta_{I,1}^2} + \frac{\partial^2 \phi(\vec{\theta}_I)}{\partial \theta_{I,2}^2} \right)\tag{11}$$

The convergence  $\kappa$  is defined as half the Laplacian of the projected gravitational potential  $\Delta \phi$ , and is directly proportional to the projected matter density of the lens (see Fig. 5). For this reason,  $\kappa$  is often referred to as the mass distribution of the lens.

The dilation and distortion of images of distant galaxies are directly related to the distribution of the (dark) matter and thus to the geometry and the dynamics of the Universe. As a consequence, weak gravitational lensing offers

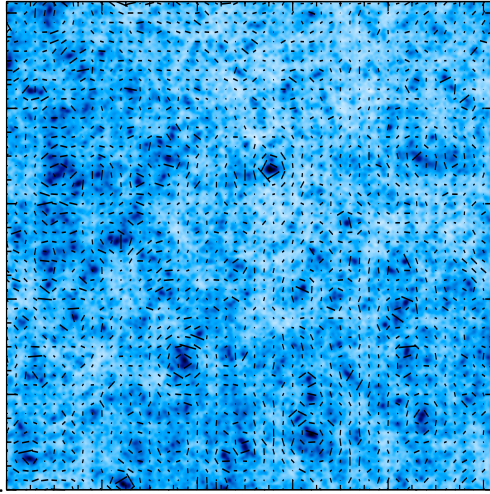


Figure 5: Simulated convergence map by [93] covering a  $2^\circ \times 2^\circ$  field with  $1024 \times 1024$  pixels. The shear map is superimposed to the convergence map. The size and the direction of the line segments represent the amplitude and the direction of the deformation locally.

unique possibilities for probing the statistical properties of dark matter and dark energy in the Universe. The weak lensing effect is typically very small, therefore the constraints that can be obtained on cosmology from the weak lensing effect rely strongly on the quality of the techniques used to analyze the data. In the following, an overview of the different techniques currently used to process weak lensing data will be presented.

### 3 Shear estimation

As described previously, the weak gravitational lensing effect distorts the images of background galaxies. The deformations can be split into two terms, the shear  $\gamma$  and the convergence  $\kappa$ . The shear term stretches the background galaxies tangentially around the foreground mass and the convergence term magnifies (or demagnifies) them by increasing (or decreasing) their size.

In this section, we describe the methods used to measure the shear field  $\gamma$ . In the next section, we will explain how the convergence field  $\kappa$  is derived from the shear field. Either the shear field or the convergence field can be used to constrain the cosmological model (see §6), but whatever the method used, the constraints on the cosmological model will depend on the shear measurement accuracy.

### 3.1 Basics

To first approximation, the gravitational shear  $\gamma$  can be traced from the ellipticity of the galaxies that can be expressed as a function of the quadrupole moments of the light distribution of the galaxy image  $M_{i,j}$ :

$$\epsilon_1 = \frac{M_{1,1} - M_{2,2}}{M_{1,1} + M_{2,2}}, \quad (12)$$

$$\epsilon_2 = \frac{2M_{1,2}}{M_{1,1} + M_{2,2}}. \quad (13)$$

where  $M_{i,j}$  are defined by:

$$M_{i,j} = \frac{\int d^2\theta W(\theta) I(\theta) \theta_i \theta_j}{\int d^2\theta W(\theta) I(\theta)}, \quad (14)$$

where  $W$  is a Gaussian function of scale length  $r$  estimated from the object size,  $I$  is the surface brightness of the object and  $\theta$  is the angular distance from the object center.

The induced shear is small, typically around an order of magnitude smaller than the RMS ellipticity seen in background galaxies, therefore the weak lensing effect cannot be measured on a single galaxy. To measure the shear field, it is necessary to measure the ellipticities of many background galaxies and construct a statistical estimate of their systematic alignment. The fundamental problem is that galaxies are not intrinsically circular, so the measured ellipticity is a combination of their intrinsic ellipticity and the gravitational shear. By assuming that the orientations of the intrinsic ellipticities of galaxies is random, any systematic alignment between multiple galaxies is assumed to be caused by gravitational lensing.

The amplitude of the cosmic shear can be quantified statistically by computing the two-point correlation functions of the shear :

$$\xi_{i,j}(\theta) = \langle \gamma_i(\vec{\theta}') \gamma_j(\vec{\theta}' + \vec{\theta}) \rangle, \quad (15)$$

where  $i, j = 1, 2$  correspond respectively to the tangential and radial component of the shear and the averaging is done over pairs of galaxies separated by angle  $\theta = |\vec{\theta}|$ . By isotropy  $\xi_{1,1}$  and  $\xi_{2,2}$  are functions only of  $\theta$  and  $\xi_{1,2} = \xi_{2,1} = 0$  is due to the scalar origin of the gravitational lensing effect and to the fact that galaxy ellipticity components are uncorrelated. This measurement demonstrates that the component of the galaxy ellipticities of well separated galaxies are uncorrelated, and it is in some sense a strong indication that our signal at small scales is of cosmological origin.

However, the weak lensing effect is so small that it requires the control of any systematic error that can mimic the lensing signal.

## 3.2 Biases

### Instrumental and atmospheric bias

A major source of systematic errors in surveys of weak gravitational lensing comes from the point spread function (PSF) due to instrumental and atmospheric effects, which causes the observed images to be smeared. Each background galaxy image is convolved by the PSF of the imagery system  $H$  to produce the image that is seen by the instrument. The point spread function (PSF) describes the response of an imaging system to a point source. For ground-based observations, atmospheric turbulence dominates the contribution to the PSF. For space-based observations, the PSF is essentially dependent on the quality of the imaging system. An ideal PSF for weak lensing observations should be small and isotropic. A large PSF tends to make small objects appear more isotropic, destroying some of the information about their true ellipticity. An anisotropic PSF adds a small level of ellipticity to observed background galaxies that can mimic a true lensing signal. Even for the most modern telescopes, the anisotropy of the PSF is usually at least of the same order of magnitude as the weak gravitational shear, and is often much larger.

PSF debiasing requires to have an estimation of the PSF at the location of each galaxy in the field. Stars present in the field (which correspond to point sources) provide a direct measurement of the PSF, and they can be used to model the variation of the PSF across the field, as long as a sufficient number of stellar images are present in the field.

Broadly, there are four groups of methods to correct for instrumental and atmospheric distortions [56] distinguished by their solution to the two most important tasks in shear estimation. The first task is how to correct for the PSF. Some methods subtract the ellipticity of the PSF from the ellipticity of each galaxy, while other methods attempt to deconvolve each galaxy from the PSF before measuring the ellipticity. The second task is how to measure the shear. Some methods do a direct measurement of the shear while others shear a model until it closely resembles the observed galaxy.

The most widely adopted method belongs to the first category, and is the result of a series of successive improvements of the original KSB method proposed by Kaiser, Squires & Broadhurst [42]. The core of the method is based on the measurement of the weighted ellipticity of the background galaxies and stars from equation 13. The PSF correction is obtained by subtracting the star weighted ellipticity  $\epsilon_i^*$  from the observed galaxy weighted ellipticity  $\epsilon_i^{obs}$ . The corrected galaxy ellipticity  $\epsilon_i$  is given by:

$$\epsilon_i = \epsilon_i^{obs} - P^{sm}(P^{sm*})^{-1}\epsilon_i^*, \quad (16)$$

where  $i=1,2$  and  $P^{sm}$  and  $P^{sm*}$  are the smear susceptibility tensors for the galaxy and star given by [42], which can be derived from higher-order moments of the images [50, 31]. This method has been used by many authors, although different interpretations of the method have introduced differences between the various implementations. One drawback of the KSB method is that for non-Gaussian PSFs, the PSF correction is poorly-defined, mathematically. In [44],

the authors propose a method to better account for realistic PSF by convolving images with an additional kernel to eliminate the anisotropic component of the PSF. Nevertheless, KSB method is thought to have reached its limits and it has been superseded by new competitive methods.

On the recent methods, some methods attempt a direct deconvolution of each galaxy from the PSF. The deconvolution requires a matrix inversion, and becomes an ill-posed inverse problem if the matrix  $H$  describing the PSF is singular (i.e. can not be inverted). The [57] shear-measurement method that belongs to a second class of methods is attempting a full deconvolution by decomposing each galaxy in shapelet basis functions convolved by the PSF. Some other methods belonging to a third class, such as [11, 49], have been developed to correct for the PSF without a direct deconvolution. These methods try to reproduce the observed galaxies by modeling each unconvolved background galaxy (the background galaxy as it would be seen without a PSF). The model galaxy is then convolved by the PSF estimated from the stars present in the field and the galaxy model tuned in such way that the convolved model reproduces the observed galaxy. Following a similar approach, the lensfit method [62, 47] measures the shear by fitting realistic galaxy profiles in a fully Bayesian way. There is a last class of methods [12] where the PSF correction is obtained by subtraction after the images have been convolved with an additional kernel to eliminate the anisotropic component of the PSF. The shear is obtained by decomposing each galaxy in a distorted shapelet basis functions.

Further improvements of these methods will be required to ensure high accuracy and reliability in a the future weak lensing studies.

### **Intrinsic alignments and correlations**

The intrinsic alignment of galaxies constitutes the major astrophysical source of systematic errors in surveys of weak gravitational lensing. Usually, the measurement of the gravitational shear is obtained by averaging the ellipticity of several nearby galaxies by assuming that the mean intrinsic ellipticity tend to zero. But in practice, the assumption of randomly distributed galaxy shapes is unrealistic. Nearby galaxies are expected to have experienced the same tidal gravitational forces, which is likely to cause a radial alignment of their intrinsic ellipticities, and therefore correlations in their observed shapes and orientations.

There are two types of intrinsic alignments. The first type of alignment appears adjacent background galaxies that form in the same large-scale gravitational potential, and which therefore share a preferred intrinsic ellipticity orientation. This is the so-called Intrinsic-Intrinsic (II) correlation (see Fig. 6).

The second type corresponds to the case where a matter structure causes a radial alignment of a foreground galaxy and contributes at the same time to the lensing signal of a background galaxy causing a tangential alignment of this background galaxy. In this case, there is an anti-correlation between the foreground intrinsic ellipticity and the background galaxy shear, known as the Gravitational-Intrinsic (GI) alignment (see Fig. 7).

Intrinsic alignments are believed to introduce a significant bias in high-precision weak lensing surveys that leads to a bias on cosmological parameters.

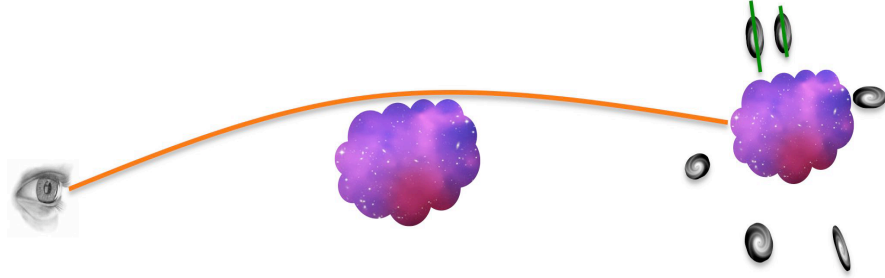


Figure 6: Intrinsic-Intrinsic alignment: When a large cloud of dark matter, gas and dust is collapsing, the surrounding matter falls in to form a disc. The resulting galaxy becomes aligned in the direction of the tidal field. Consequently, the intrinsic ellipticity of nearby galaxies will be aligned with the local tidal field like the two galaxies in green.

For example, the shear power spectrum  $P_\gamma(l)$  which is the most common method for constraining cosmological parameters, is biased by the previously described intrinsic alignments:

$$P_\gamma(l) = P_\gamma^{GG}(l) + P_\gamma^{II}(l) + P_\gamma^{GI}(l) \quad (17)$$

where the first term is the usual gravitational lensing contribution, the second term arises from the intrinsic alignment of physically close galaxies and the last term arises from Gravitational-Intrinsic alignments.

The shear power spectrum  $P_\gamma(l)$  is the Fourier transform of the shear two-point correlation  $\xi_{i,j}(\theta)$  defined in the previous section.

The use of galaxy distance information, obtained from either photometric or spectroscopic redshifts<sup>1</sup>, can be used to reduce these systematic errors. In studies [56, 75], the signal is evaluated as a function of the galaxy redshift, thanks to the photometric redshift information. But the cosmological constraints in these recent papers have been calculated assuming there are no intrinsic alignments, although the bias is non-negligible. To increase the precision of future surveys, it is essential to eliminate intrinsic alignments. It has been shown [28, 45, 46, 88] that the Intrinsic-Intrinsic correlations can be almost completely removed by identifying physically close pairs of galaxies and applying a weighting scheme based on photometric redshifts. The Gravitational-Intrinsic effect is more problematic as it affects pairs of galaxies which are not physically close. There are two main approaches to deal with GI alignments. The first approach is model-independent; it is a purely geometrical method that removes the GI effect by using a particular linear combination of tomographic shear power spectra, assuming the redshifts of the galaxies are known [40, 41]. The other approach

<sup>1</sup>Photometric and spectroscopic redshifts are estimates for the distance of an astronomical object such as a galaxy. The photometric redshift measurement uses the brightness of the object viewed through various standard filters while the spectroscopic redshift measurement is obtained from the spectroscopic observation of an astronomical object.

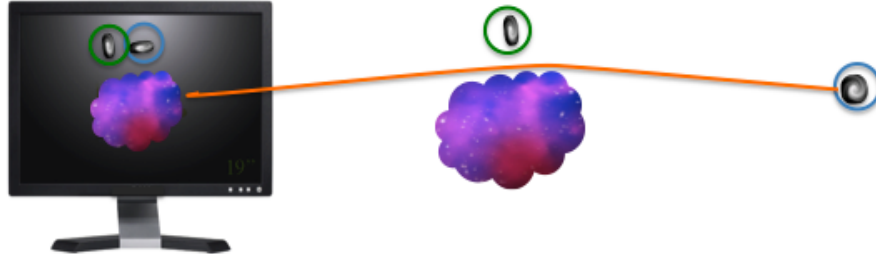


Figure 7: Gravitational-Intrinsic alignment: When the tidal field generated by a (dark) matter structure aligns a foreground galaxy (in green) and at the same time generates a gravitational shear on a background galaxy (in blue), there is an anti-correlation between the intrinsic ellipticity of a foreground galaxy (in green, in the screen) and the gravitational shear of a background galaxy (in blue, in the screen).

tries to model the expected intrinsic alignment contribution for a particular survey. The parameters of the model can thus be varied and marginalized over to constrain cosmological parameters [13, 10, 39].

### 3.3 Challenges

All methods involve estimating an ellipticity  $\epsilon_i$  for each galaxy, whose definition can vary between the different methods. The accuracy of the shear measurement method depends on the technique used to estimate the ellipticity of the galaxies in the presence of observational and cosmological effects. In the KSB method [42], the ellipticity is derived from quadrupole moments weighted by a Gaussian function. This method has been used by many authors but it is not sufficiently accurate for future surveys. The extension of KSB to higher-order moments has been done to allow more complex galaxy and PSF shapes [14, 11, 49]. The shapelets (see [58]) can be seen as an extension of KSB to higher-order; the first few shapelet basis functions are precisely the weighted functions used in KSB. However, shapelet basis functions are constructed from Hermite polynomials weighted by a Gaussian function and are not optimal to represent galaxy shapes that are closer to exponential functions. By consequence, in the presence of noise, shear measurement methods based on a shapelet decomposition are not optimal.

Many other methods have been developed to address the global problem of the shear estimation. To prepare for the next generation of wide-field surveys, a wide range of shear estimation methods have been compared blindly in the Shear Testing Program (STEP) ([29, 56]). Several methods have achieved an accuracy of a few percent. However, the accuracy required for future surveys is of the order of 0.1%. Another challenge, called GREAT08 ([15]), has been set outside the weak lensing community as an effort to spur further developments. The primary goal was to stimulate new ideas by presenting the problem to

researchers outside the shear measurement community. A number of fresh ideas have emerged, especially to reduce the dependence on realistic galaxy modelling. The most successful astronomical algorithm has been found to be the lensfit method [62, 47]. In the upcoming GREAT10 challenge, the image simulations will become more sophisticated and complex, in order to further improve the accuracy of the methods.

## 4 2D mapping of the dark matter

The problem of mass reconstruction has become a central topic in weak lensing since the very first maps have demonstrated that this method can be used to visualize the dark side of the Universe. Indeed, weak gravitational lensing provides a unique way to map directly the distribution of dark matter in the Universe. This is done by estimating the convergence  $\kappa$ , which is directly proportional to the projected matter distribution along the line of sight.

### 4.1 Inversion problem

The convergence, which corresponds to the isotropic distortion of background galaxies images, is not easy to estimate directly because the initial size of galaxies is not known. However, the convergence  $\kappa$  can be derived by inversion of the shear field. In order to do this, a shear field averaged on a regular grid is required. The grid needs to be sufficiently coarse that several galaxies fall in each cell of the grid, otherwise the shear field is only defined on an irregular grid defined by the galaxy positions, yet not so coarse that the shear changes sufficiently across the grid cell.

#### Global inversion

A global relation between  $\kappa$  and  $\gamma$  can be derived from the relations (9) and (10). Indeed, it has been shown by [43] that the least square estimator  $\hat{\kappa}_n$  of the convergence  $\hat{\kappa}$  in the Fourier domain is:

$$\hat{\kappa}_n(k_1, k_2) = \hat{P}_1(k_1, k_2)\hat{\gamma}_1^{obs}(k_1, k_2) + \hat{P}_2(k_1, k_2)\hat{\gamma}_2^{obs}(k_1, k_2), \quad (18)$$

where  $\gamma_1^{obs}$  and  $\gamma_2^{obs}$  represent the noisy shear components. The hat symbols denote the Fourier transform and:

$$\begin{aligned} \hat{P}_1(k_1, k_2) &= \frac{k_1^2 - k_2^2}{k_1^2 + k_2^2} \\ \hat{P}_2(k_1, k_2) &= \frac{2k_1k_2}{k_1^2 + k_2^2}, \end{aligned} \quad (19)$$

with  $\hat{P}_1(k_1, k_2) \equiv 0$  when  $k_1^2 = k_2^2$ , and  $\hat{P}_2(k_1, k_2) \equiv 0$  when  $k_1 = 0$  or  $k_2 = 0$ . The most important drawback of this method is that it requires a convolution of shears to be performed over the entire sky. As a result, if the observed shear field has a finite size or a complex geometry, the method can produce artifacts on

the reconstructed convergence distribution near the boundaries of the observed field. Masking out the bright stars in the field is common practice in weak lensing analysis, therefore the global inversion requires to proper treatment of the gaps in the shear map.

### Local inversion

There exist local inversions, which have the advantage to address the problems encountered by global relations: the missing data problem and the finite size of the field. A relation between the gradient of  $K = \log(1 - \kappa)$  and combinations of first derivatives of  $g = \frac{\gamma}{1 - \kappa}$  have been derived by [42] :

$$\frac{-1}{1 - |g|^2} \begin{pmatrix} 1 - g_1 & -g_2 \\ -g_2 & 1 + g_1 \end{pmatrix} \begin{pmatrix} g_{1,1} + g_{2,2} \\ g_{2,1} - g_{1,2} \end{pmatrix} \equiv u \quad (20)$$

This equation can be solved by line integration and there exist an infinite number of local inverse formulae which are exact for ideal data on a finite-size field, but which differ in their sensitivity to observational effects such as noise. The reason why different schemes yield different results can be understood by noting that the vector field  $u$  (the right-hand side of equation 20) contains a rotational component due to noise because it comes from observational estimates. In [79], the authors have split the vector field  $u$  into a gradient part and a rotational part and they derive the best formula that minimizes the sensitivity to observational effects by convolving the gradient part of the vector field  $u$  with a given kernel.

The local inversions reduce the unwanted boundary effects but whichever the formula is used, the reconstructed field will be more noisy than that obtained with a global inversion. Note also that the reconstructed dark matter mass map still has a complex geometry that will complicate the later analysis.

## 4.2 E and B modes decomposition

Just as a vector field can be decomposed into a gradient or electric (E) component, and a curl or magnetic (B) component, the shear field  $\gamma_i(\theta)$  can be decomposed into two components which for convenience we also call (E) and (B). The decomposition of the shear field into each of these components can be easily performed by noticing that a pure E mode can be transformed into a pure B mode by a rotation of the shear by  $45^\circ$ :  $\gamma_1 \rightarrow -\gamma_2$ ,  $\gamma_2 \rightarrow \gamma_1$ .

Because the weak lensing arises from a scalar potential (the Newtonian potential  $\Phi$ ), it can be shown that weak lensing only produces E modes. As a result, the least square estimator of the E mode convergence field is simply:

$$\tilde{\kappa}^{(E)} = \frac{\partial_1^2 - \partial_2^2}{\partial_1^2 + \partial_2^2} \gamma_1 + \frac{2\partial_1\partial_2}{\partial_1^2 + \partial_2^2} \gamma_2, \quad (21)$$

On the other hand, residual systematics arising from imperfect correction of the instrumental PSF, telescope aberrations or complex geometry, generally

generates both E and B modes. The presence of B modes can thus be used to test for the presence of residual systematic effects in current weak lensing surveys.

### 4.3 Missing data

As mentioned previously, analyzing an image for weak lensing inevitably involves the masking out of regions to remove bright stars from the field. The measured shear field is then incomplete. Although the masking out of the stars is common practice, depending on the tools used to analyze this incomplete field, the gaps present in the field will require proper handling.

At present, the majority of lensing analyses use the two-point statistics of the cosmic shear field introduced §3.1 because this method is not biased by missing data. However, this method is computationally intensive and could not be used for future ultra wide lensing surveys. Measuring the power spectrum is significantly less demanding computationally, but is strongly affected by missing data. Higher-order statistical measures of the cosmic shear field, such as three or four-point correlation functions have been studied and have shown to provide additional constraints on cosmological parameters but could not be reasonably estimated in future survey.

A solution that has been proposed by [67] to deal with missing data consists in judiciously filling in the masked regions by using an “inpainting” method simultaneously with a global inversion. Inpainting techniques are methods by which an extrapolation of the missing information is carried out using some priors on the solution. This new method uses a prior of sparsity in the solution introduced by [22]. It assumes that there exists a dictionary ( i.e. a representation)  $\mathcal{D}$  in which the complete data are sparse whilst the incomplete data are less sparse. This means that we seek a dictionary  $\alpha = \Phi^T X$  of the signal  $X$  in the representation  $\Phi$  where most coefficients  $\alpha_i$  are close to zero, while only a few have a significant absolute value. If the signal is a sinusoid, its sparsest representation will be the Fourier representation because the signal can be represented by a unique coefficient in the Fourier domain. In many applications - such as compression, denoising, source separation and, of course, inpainting - a sparse representation of the signal is necessary to improve the quality of the processing. Over the past decade, traditional signal representations have been replaced by a large number of new multiresolution representations. Instead of representing signals as a superposition of sinusoids using classical Fourier representation, we now have many available alternative representations such as wavelets [53], ridgelets [18] or curvelets [84, 17], most of which are overcomplete. This means that some elements of the dictionary can be described in terms of other ones, therefore a signal decomposition in such a dictionary is not unique. Although this can increase the complexity of the signal analysis, it gives us the possibility to select among many possible representations the one which gives the sparsest representation of our data.

The weak lensing inpainting method consists in recovering a complete convergence map  $\kappa$  from the incomplete measured shear field  $\gamma_i^{obs}$ . The solution is

obtained by minimizing:

$$\min_{\kappa} \|\mathcal{D}^T \kappa\|_0 \text{ subject to } \sum_i \|\gamma_i^{obs} - M(P_i * \kappa)\|^2 \leq \sigma, \quad (22)$$

where  $P_i$  is defined by the relation 20,  $\mathcal{D}^T$  is the DCT (Digital Cosine Transform),  $\sigma$  stands for the noise standard deviation and  $M$  is the binary mask (i.e.  $M_i = 1$  if we have information at pixel  $i$ ,  $M_i = 0$  otherwise). We denote by  $\|z\|_0$  the  $l_0$  pseudo-norm, i.e. the number of non-zero entries in  $z$ , and by  $\|z\|$  the classical  $l_2$  norm (i.e.  $\|z\|^2 = \sum_k (z_k)^2$ ).

If  $\mathcal{D}^T \kappa$  is sparse enough, the  $l_0$  pseudo-norm can be replaced by the convex  $l_1$  norm (i.e.  $\|z\|_1 = \sum_k |z_k|$ ) [21]. The solution of such an optimization task can be obtained through an iterative thresholding algorithm called MCA (Morphological Component Analysis) [22]:

$$\kappa^{n+1} = \Delta_{\mathcal{D}, \lambda_n} (\kappa^n + M[P_1 * (\gamma_1^{obs} - P_1 * \kappa^n) + P_2 * (\gamma_2^{obs} - P_2 * \kappa^n)]), \quad (23)$$

where the nonlinear operator  $\Delta_{\mathcal{D}, \lambda}(Z)$  consists in:

- decomposing the signal  $Z$  on the dictionary  $\mathcal{D}$  to derive the coefficients  $\alpha = \mathcal{D}^T Z$ .
- threshold the coefficients with a hard-thresholding ( $\tilde{\alpha} = \alpha_i$  if  $|\alpha_i| > \lambda_n$  and 0 otherwise). The threshold parameter  $\lambda_n$  decreases with the iteration number.
- reconstruct  $\tilde{Z}$  from the thresholded coefficients  $\tilde{\alpha}$ .

The MCA algorithm has been originally designed for the separation of linearly combined texture and cartoon layers in a given image. By incorporating a binary mask in the model, it leads to an inpainting method. MCA relies on an iterative thresholding algorithm, using a threshold which decreases linearly towards zero along the iterations. This algorithm requires to perform at each iteration a forward transform, a thresholding of the coefficients and an inverse transform.

This method enables to reconstruct a complete convergence map  $\kappa$  that can be used to perform further analyses of the field. The method can also be used to reconstruct the dark matter distribution and do comparisons with other probes. These comparisons are usually done after a filtering of the dark matter map, whose quality is improved by the absence of missing data.

#### 4.4 Filtering

The convergence map obtained by inversion of the shear field is very noisy (infinite variance) [43] even with a global inversion. The noise comes from the shear measurement errors and the residual intrinsic ellipticities present in the shear maps that propagate during the weak lensing inversion. An efficient filtering is

required to map the dark matter and to compare its distribution with other probes.

### Linear filters

Linear filters are often used to eliminate or attenuate unwanted frequencies.

- Gaussian filter:  
The standard method [43] consists in convolving the noisy convergence map  $\kappa$  with a Gaussian window  $G$  with standard deviation  $\sigma_G$ :

$$\kappa_G = G * \kappa_n = G * P_1 * \gamma_1^{obs} + G * P_2 * \gamma_2^{obs}. \quad (24)$$

The Gaussian filter is used to suppress the high frequencies of the signal. However, a major drawback of this method is that the quality of the result depends strongly on the value of the width  $\sigma_G$  of the Gaussian filter, which controls the level of smoothing.

- Wiener filter:  
An alternative to Gaussian filter is the Wiener filter [3, 92] obtained by assigning the following weight to each  $k$ -mode:

$$w(k_1, k_2) = \frac{|\hat{\kappa}(k_1, k_2)|^2}{|\hat{\kappa}(k_1, k_2)|^2 + |\hat{N}(k_1, k_2)|^2}. \quad (25)$$

In theory, if the noise and the signal follow a Gaussian distribution, the Wiener filter provides the minimum variance estimator. However, the signal is not Gaussian. In fact, on small scales, the convergence map deviates significantly from gaussianity. However, the Wiener filter leads to reasonable results, with a better resolution than a simple Gaussian filter.

Linear filters are very common and easy to design, but improved results can be obtained using non-linear filtering.

### Bayesian methods

- Bayesian filters  
Some recent filters are based on the Bayesian theory that considers that some prior information can be used to improve the solution. Bayesian filters search for a solution that maximizes the a posteriori probability using Bayes' theorem :

$$P(\kappa|\kappa_n) = \frac{P(\kappa_n|\kappa)P(\kappa)}{P(\kappa_n)}, \quad (26)$$

where :

- $P(\kappa_n|\kappa)$  is the likelihood of obtaining the data  $\kappa_n$  given a particular convergence distribution  $\kappa$ .

- $P(\kappa_n)$  is the a priori probability of the data  $\kappa_n$ . This term, called the evidence, is simply a constant that ensures that the a posteriori probability is correctly normalized.
- $P(\kappa)$  is the a priori probability of the estimated convergence map  $\kappa$ . This term codifies our expectations about the convergence distribution before acquisition of the data  $\kappa_n$ .
- $P(\kappa|\kappa_n)$  is called the a posteriori probability.

Searching for a solution that maximizes  $P(\kappa|\kappa_n)$  is the same that searching for a solution that minimizes the quantity  $\mathcal{Q}$  :

$$\begin{aligned}\mathcal{Q} &= -\log(P(\kappa|\kappa_n)), \\ \mathcal{Q} &= -\log(P(\kappa_n|\kappa)) - \log(P(\kappa)).\end{aligned}\tag{27}$$

If the noise is uncorrelated and follows a Gaussian distribution, the likelihood term  $P(\kappa_n|\kappa)$  can be written:

$$P(\kappa_n|\kappa) \propto \exp\left(-\frac{1}{2}\chi^2\right),\tag{28}$$

with :

$$\chi^2 = \sum_{x,y} \frac{(\kappa_n(x,y) - \kappa(x,y))^2}{\sigma_{\kappa_n}^2}.\tag{29}$$

Equation (28) can then be expressed as follows:

$$\mathcal{Q} = \frac{1}{2}\chi^2 - \log(P(\kappa)) = \frac{1}{2}\chi^2 - \beta H,\tag{30}$$

where  $\beta$  is a constant that can be seen as a parameter of regularization and  $H$  represents the prior that is added to the solution.

If we have no expectations about the convergence distribution, the a priori probability  $P(\kappa)$  is uniform and the maximum a posteriori is equivalent to the well-known maximum likelihood. This maximum likelihood method has been used by [5, 81] to reconstruct the weak lensing field, but the solution needs to be regularized in some way to prevent overfitting the data. This has been done via the a priori probability of the convergence distribution. The choice of this prior is one of the most critical aspects of the Bayesian analysis. An Entropic prior is frequently used but there exists many definitions of the Entropy [25]. One that is currently used is the Maximum Entropy Method (MEM) [16, 55].

Some authors [5, 80] have also suggested to reconstruct the gravitational potential  $\phi$  instead of the convergence distribution  $\kappa$ , still using a Bayesian approach, but it is clearly better to reconstruct the mass distribution  $\kappa$  directly because it allows a more straightforward evaluation of the uncertainties in the reconstruction.

- Multiscale Bayesian filters

A multiscale maximum entropy prior has been proposed by [55] which uses the intrinsic correlation functions (ICF) with varying width. The multichannel MEM-ICF method consists in assuming that the visible-space image  $I$  is formed by a weighted sum of the visible-space image channels  $I_j$ ,  $I = \sum_{j=1}^{N_c} p_j I_j$  where  $N_c$  is the number of channels and  $I_j$  is the result of the convolution between a hidden image  $h_j$  with a low-pass filter  $C_j$ , called the ICF (Intrinsic Correlation Function) (i.e.  $I_j = C_j * o_j$ ). In practice, the ICF is a Gaussian. The MEM-ICF constraint is:

$$H_{ICF} = \sum_{j=1}^{N_c} |o_j|^{-m_j} |o_j| \log \left( \frac{|o_j|}{m_j} \right). \quad (31)$$

Another approach, based on the sparse representation of the data, has been used by [65] that consists in replacing the standard Entropy prior by a wavelet-based prior. Sparse representations of signals have received a considerable interest in recent years. The problem solved by the sparse representation is to search for the most compact representation of a signal in terms of linear combination of atoms in an overcomplete dictionary.

The entropy is now defined as :

$$H(I) = \sum_{j=1}^{J-1} \sum_{k,l} h(w_{j,k,l}). \quad (32)$$

In this approach, the information content of an image  $I$  is viewed as the sum of the information at different scales  $w_j$  of a wavelet transform. The function  $h$  defines the amount of information relative to a given wavelet coefficient. Several functions have been proposed for  $h$ .

In [85], the most appropriate entropy for the weak lensing reconstruction problem has been found to be the NOISE-MSE entropy:

$$h(w_{j,k,l}) = \frac{1}{\sigma_j^2} \int_0^{|w_j|} u \operatorname{erfc} \left( \frac{|w_{j,k,l}| - u}{\sqrt{2}\sigma_j} \right) du, \quad (33)$$

where  $\sigma_j$  is the noise standard deviation at scale  $j$ . The NOISE-MSE exhibits a quadratic behavior for small coefficients and is very close to the  $l_1$  norm (i.e. the absolute value of the wavelet coefficient) when the coefficient value is large, which is known to produce good results for the analysis of piecewise smooth images.

A Multiscale Bayesian filter, called MRLens (Multi-Resolution for weak Lensing) [85], based on the above method, has shown to outperform other techniques (Gaussian, Wiener, MEM, MEM-ICF) in the reconstruction of dark matter. It has been used to reconstruct the largest weak lensing survey ever undertaken with the Hubble Space Telescope [59]. The result is shown Fig. 8, this map is

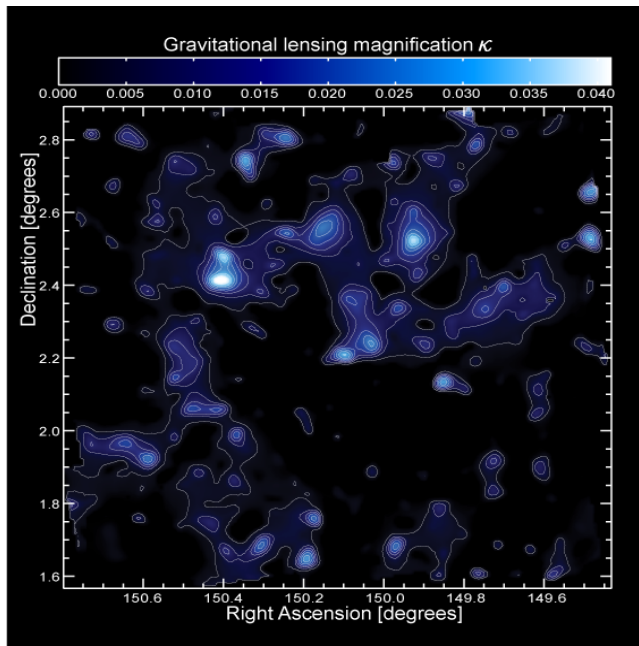


Figure 8: Map of the dark matter distribution in the 2-square degrees COSMOS field by [59]: the linear blue scale shows the convergence field  $\kappa$ , which is proportional to the projected mass along the line of sight. Contours begin at 0.004 and are spaced by 0.005 in  $\kappa$ .

the most precise and detailed dark matter mass map, covering a large enough area to see extended filamentary structures.

In the paper [92], a study using a simulated full-sky weak lensing map has shown that the Wiener filter is optimal to filter the large-scale structures but not the non-Gaussian structures such as the clusters. On the contrary, the MRLens filter is very efficient to reconstruct the clusters but not the large-scale structures. From these results, the authors indicate that an optimal method could be obtained by a smart combination of these two filters.

## 5 3D mapping of the dark matter

In this section, we will discuss methods to reconstruct the 3D dark matter field from shear measurements.

### 5.1 Formalism

Following the flat-sky approach, the 3D convergence field can be reconstructed by sorting the galaxies in several redshift bins. A convergence map can be com-

puted from the shear at each redshift bin using the relation 18. But, this reconstruction is unsatisfactory because there are correlations between the convergence maps reconstructed at different redshift bins. The reconstruction of a 3D dark matter map without correlations requires to estimate the 3D density contrast  $\delta$  or the 3D gravitational potential  $\Phi$ , which is related to the density contrast  $\delta$  by Poisson's equation:

$$\nabla^2\Phi = 4\pi G\rho_m\delta a^2 = \frac{3}{2}\lambda_H^{-2}\Omega_m a^{-1}\delta, \quad (34)$$

where  $a$  is the cosmological scale factor,  $\delta = (\rho - \bar{\rho})/\bar{\rho}$  is the density contrast,  $\lambda_H = 1/H_0$  is the Hubble length and  $\Omega_m$  is the present-day mass-density parameter.

The 3D gravitational potential  $\Phi$  can be reconstructed using the weak lensing measurements together with the redshifts for all galaxies of the field [90, 89, 3, 27, 91]. Indeed, assuming the Born approximation (i.e. assuming the light path is unperturbed), the lensing potential  $\phi$  is given by :

$$\phi(r) = 2 \int_0^r dr' \left( \frac{f_K(r) - f_K(r')}{f_K(r)f_K(r')} \right) \Phi(r'), \quad (35)$$

where  $f_K(r)$  is the angular diameter distance, which is a function of the comoving radial distance  $r$  and the curvature  $K$ . This relation may be inverted to yield [90]:

$$\Phi(r) = \frac{1}{2}\partial_r r^2 \partial_r \phi(r). \quad (36)$$

But the lensing potential  $\phi$  is not an observable. The observable is the reduced shear  $g_i(\theta) = \frac{\gamma_i(\theta)}{1-\kappa(\theta)}$ . In the weak lensing regime,  $\kappa$  can be neglected and the observable becomes the shear  $\gamma_i$  corresponding to the distortion of the lensed images of background galaxies.

An estimate of the lensing potential  $\tilde{\phi}$  from the shear field is given by the following relation [43]:

$$\tilde{\phi}(\mathbf{r}) = 2\partial^{-4}\partial_i\partial_j\gamma_{ij}(\mathbf{r}) \quad (37)$$

with  $\gamma_{ij} = \begin{pmatrix} \gamma_1 & \gamma_2 \\ \gamma_2 & -\gamma_1 \end{pmatrix} = (\partial_i\partial_j - \frac{1}{2}\delta_{ij}\partial^2)\phi$  is the shear matrix.

The lensing potential  $\phi$  is related to the convergence field by the following relation :

$$\nabla^2\phi = 2\kappa(\theta) \quad (38)$$

The density contrast  $\delta$  is related to the convergence  $\kappa$  by a line of sight integral over the lensing efficiency function  $\bar{W}$ :

$$[\kappa^i]_k = \frac{3H_0^2}{2c^2}\Omega_m \int_0^\infty dr \frac{\bar{W}^i(r)f_K(r)}{a(r)}\delta(f_K(r)\theta_k, r),$$

$$\bar{W}^i(r) = \int_0^\infty dr' \frac{f_K(r' - r)}{f_K(r')} \left[ p_z^{(i)}(z) \frac{dz}{dr} \right]_{z=z(r')}, \quad (39)$$

with  $p_z^i$  represents the  $i$ th bin of the probability distribution of sources as a function of redshift.

With these sets of equations the 3D lensing potential, the 3D gravitational potential, the 3D convergence and the 3D matter density fields can all be generated from combined shear and redshift information.

Some authors have attempted to reconstruct the 3D lensing potential or the 3D gravitational potential [3, 59] in order to reconstruct the 3D matter density field. But in the majority of papers relating to 3D lens mapping [35, 83, 95], the reconstruction of the 3D matter density field is derived from the convergence tomography. It consists in two linear steps: a 3D convergence field is first derived from the shear measurements sorted in several redshift bins using the relation 18; then, the 3D density contrast is obtained by inversion of the relation 39. The resulting reconstruction is very noisy and requires a regularization of the solution.

## 5.2 Filtering

Linear map-making can be expressed in terms of the general inverse problem:

$$d_b = P_{ba} s_a + n_b \quad (40)$$

where we seek an estimate  $\hat{s}_a$  from a data vector  $d_b$  that is a linear projection  $P_{ba}$  of the signal with measurement noise  $n_b$ .  $s_a$  can be the 3D density contrast or the 3D gravitational potential and  $d_b$  can be the 3D shear field or the 3D convergence field.

### Linear filters

A first linear approach is the maximum likelihood that searches for an estimate of the signal  $\hat{s}_a$  that minimizes  $\chi^2$ :

$$\chi^2 = (d_b - P_{ba} \hat{s}_a)^t N_{bb}^{-1} (d_b - P_{ba} \hat{s}_a), \quad (41)$$

where  $N_{bb}$  is the noise covariance. Minimizing  $\chi^2$  returns the linear estimator:

$$\hat{s}_a = R_{ab} d_b, \quad (42)$$

where :

$$R_{ab} = [P_{ba}^t N_{bb}^{-1} P_{ba}]^{-1} P_{ba}^t N_{bb}^{-1}. \quad (43)$$

If  $P_{ba}$  is invertible then  $R_{ab} = P_{ba}^{-1}$  and the estimator becomes independent of both the signal and the noise. Note that minimizing  $\chi^2$  is not the same as minimizing the reconstruction noise  $N_{aa} = \langle (\hat{s}_a - s_a)(\hat{s}_a - s_a)^t \rangle$ . It minimizes  $N_{aa}$  subject to the constraint  $R_{ab} P_{ba} = I$

A Bayesian approach can be used to set a penalty function  $H$  on the solution using prior knowledge of the statistical properties of the signal and the noise. An estimate of the signal can then be sought by minimizing  $\chi^2 + H$ . Defining the penalty function  $H = \hat{s}_w^t S_{aa}^{-1} \hat{s}_w$ , the minimization of  $\chi^2 + H$  returns the Wiener filtered estimate of the signal  $\hat{s}_w = R_{wb} d_b$ , where:

$$\begin{aligned} R_{wb} &= [S_{aa}^{-1} + P_{ba}^t N_{bb}^{-1} P_{ba}]^{-1} P_{ba}^t N_{bb}^{-1} \\ R_{wb} &= S_{aa} P_{ba}^t [P_{ba} S_{aa} P_{ba}^t + N_{bb}]^{-1}. \end{aligned} \quad (44)$$

The classical Wiener filter definition (see equation 25) can be recovered by assuming the data may be expressed as  $d_b = I s_a + n_b$ . Equation 45 then becomes:

$$R_{wb} = S_{aa} [S_{aa} + N_{bb}]^{-1}, \quad (45)$$

where  $S_{aa} = \langle s_a s_a^t \rangle$  and  $N_{bb} = \langle n_b n_b^t \rangle$ . The Wiener filter reduces the reconstruction noise  $N_{aa}$  by using the expected noise properties as a prior on the solution [35].

In the literature, no 3D Wiener filter have yet been proposed to process the full 3D matter density field. In [35], the authors apply a Wiener filter along each individual line-of-sight, ignoring the correlation between different line of sights (radial Wiener filter). In [83], the authors use two types of pseudo-3D Wiener filter: a ‘‘radial Wiener filter’’ and a ‘‘transverse Wiener filter’’. Both filters are well adapted to filter the large-scale regime because the signal is Gaussian, but small scales require a more efficient filtering. Moreover, both filters show a systematic shift and stretch of the structures in the radial direction, and fail to account for correlations either along the line of sight (transverse filter) or in the transverse direction (radial filter).

### Non-Linear filters

Several non-linear filters have been proposed to filter the 3D matter density field. The MEM filter that has been presented in section 4.4 has been introduced by [35] to reconstruct dark matter halos in 3D matter distribution. The MEM filter that is based on the Bayesian theory has already been applied in 2D matter distribution (see [16, 55]). In this filter the penalty function is an entropy that is estimated from the full 3D weak lensing field. A fundamental problem with the MEM filter is the difficulty in assessing the errors in the reconstruction.

Another non-linear approach that is a full-3D filter has been proposed by [35, 95], and consists in expressing the data in a new set of uncorrelated orthogonal basis elements that are ranked by their signal-to-noise ratio. This method is known as the Karhunen-Loeve transform or Singular Value Decomposition, assuming the modes are the eigenvectors of the covariance matrix. A direct noise reduction which does not require knowledge of the statistical properties of the signal is obtained by eliminating the lower signal-to-noise singular values.

The full reconstruction of the 3D dark matter distribution from weak lensing has only been considered recently [35, 89] because the finite size of the earlier

surveys did not allow for 3D mapping. Recently, the COSMOS survey [59, 60] has enabled to reconstruct the first 3D weak lensing map. Although the results were limited by the finite size of the survey, they provide a framework for future large weak lensing surveys like the future Euclid mission. The next step, is to develop a full 3D Wiener filter, to extend the MRLens method from 2D to 3D, and possibly to develop a combined filtering method.

## 6 Cosmological model constraints

Measurement of the distortions in images of background galaxies caused by large-scale structures provides a direct way to study the statistical properties of the evolution of structures in the Universe. Weak gravitational lensing measures the mass and can thus be directly compared to theoretical models of structure formation. But because we have only one realization of our Universe, a statistical analysis is required to do the comparison. The estimation of the cosmological parameters from weak lensing data can be seen as an inverse problem. The direct problem consisting of deriving weak lensing data from cosmological parameters can be solved using numerical simulations, but the inverse problem cannot be solved so easily because the N-body equations used by the numerical simulations can not be inverted.

### 6.1 Methodology

A solution is to use analytical predictions for statistics of cosmic shear and to compare with the values estimated from the data. A statistical analysis of the weak lensing field is then required to constrain the cosmological parameters.

The method that is usually used to constrain cosmological parameters from statistic estimation is the maximum likelihood (see §4.4). Let's estimate the statistic  $\eta(x, y)$  in the weak lensing field to constrain the cosmological parameters  $p_1$  and  $p_2$ . By assuming the noise follows an uncorrelated and Gaussian distribution, the likelihood function  $\mathcal{L}$  is defined as follows:

$$\mathcal{L}(p_1, p_2, p_3) \equiv P(\eta^{obs} | \eta^{mod}) \propto \exp\left(-\frac{1}{2}\chi^2(p_1, p_2, p_3)\right), \quad (46)$$

with:

$$\chi^2(p_1, p_2, p_3) = \sum_{x,y} \frac{(\eta^{obs}(x, y) - \eta^{mod}(x, y; p_1, p_2, p_3))^2}{\sigma^2(x, y)}, \quad (47)$$

where  $\eta^{mod}$  is the analytic prediction depending on the two cosmological parameters  $(p_1, p_2)$  and a nuisance parameter  $(p_3)$ .  $\eta^{obs}$  is the statistic estimation from the data.  $\chi^2$  is then a function of three parameters. A two-dimensional probability distribution can be obtained by marginalizing the three-dimensional probability distribution function over  $p_3$ :

$$\mathcal{L}(p_1, p_2) = \int dp_3 P(p_3) \exp\left(-\frac{1}{2}\chi^2(p_1, p_2, p_3)\right), \quad (48)$$

Here  $P(p_3)$  is the prior distribution function for the parameter  $p_3$ , which is assumed to be a known Gaussian distribution. Using  $\mathcal{L}(p_1, p_2)$ , we can define the 1, 2 and  $3\sigma$  contours on the two-dimensional  $(p_1, p_2)$  parameter space. The best-fit values for  $p_1$  and  $p_2$  can also be easily determined by maximizing the likelihood function. Recent cosmic shear results obtained from maximum likelihood maximization are given in [24, 76].

The different cosmological parameters can be quantified using a variety of statistics estimated either in the shear field or in the convergence field. Most lensing studies do the statistical analysis in the shear field to avoid the inversion. But most of the following statistics can also be estimated in the convergence field if the missing data are carefully accounted for. A description of the different statistics that can be used to constrain cosmological parameters is provided below.

## 6.2 Second-order statistics

The most common method for constraining cosmological parameters uses second-order statistics of the shear field calculated either in real or Fourier space (or Spherical Harmonic space). Whatever the second-order statistic that is considered, it can be easily related to the theoretical 3D matter power spectrum  $P(k, \chi)$  by means of the 2D convergence power spectrum  $P_\kappa(l)$ .

- The convergence and shear power spectra  $P_\kappa(l)$  and  $P_\gamma(l)$ :  
The 2D convergence power spectrum  $P_\kappa(l)$  only depends on  $l = |\vec{l}|$ , and is defined by:

$$\langle \hat{\kappa}(\vec{l}) \hat{\kappa}(\vec{l}') \rangle = (2\pi)^2 \delta(\vec{l} - \vec{l}') P_\kappa(l), \quad (49)$$

where  $\hat{\kappa}$  is the Fourier transform of the 2D convergence  $\kappa$ .

The 2D convergence power spectrum  $P_\kappa(l)$  can be expressed as a function of the 3D matter power spectrum  $P(k, \chi)$ , the mass fluctuations  $\delta\rho/\rho$  and cosmological parameters [68]:

$$P_\kappa(l) = \frac{9}{16} \left( \frac{H_0}{c} \right)^4 \Omega_m^2 \int d\chi \left[ \frac{g(\chi)}{a r(\chi)} \right]^2 P\left(\frac{l}{r}, \chi\right), \quad (50)$$

where  $a$  is the cosmological scale factor,  $H_0$  is the Hubble constant,  $\Omega_m$  is the matter density parameter,  $\chi$  the comoving distance,  $r = a^{-1} D_A$  with  $D_A$  being the angular diameter distance and  $g$  the lensing efficiency function.

Furthermore, in the case of weak lensing, the power spectra for the shear  $P_\gamma(l)$  and the convergence  $P_\kappa(l)$  are the same.

In general there are advantages for cosmological parameter estimation in using Fourier (or Spherical harmonic) statistics, because the Fast Fourier Transform (FFT) algorithm can be used to estimate these power spectra rapidly, and the correlation properties are more convenient to express in

Fourier space. However, for surveys with complicated geometry due to the removal of bright stars, the spatial stationarity is not satisfied and the missing data need proper handling. The problem of power spectrum estimation from weak lensing data with missing data has been studied by [30]. But real space statistics are largely used because they are easier to estimate, although statistical error bars are harder to estimate.

- Shear variance  $\langle \gamma^2(\theta) \rangle$  :

An example of real space second-order statistic is the shear variance  $\langle \gamma^2(\theta) \rangle$ , defined as the variance of the average shear  $\bar{\gamma}$  evaluated in circular patches of varying radius  $\theta_s$ . The shear variance  $\langle \gamma^2(\theta) \rangle$  can be related to the underlying 3D matter power spectrum via the 2D convergence power spectrum  $P_\kappa$  by the following relation:

$$\langle \gamma^2(\theta) \rangle = \int \frac{dl}{2\pi} l P_\kappa(l) \frac{J_1^2(l\theta_s)}{(l\theta_s)^2}, \quad (51)$$

where  $J_n$  is the Bessel function of order  $n$ . The shear variance has been frequently used in weak lensing analysis to constrain cosmological parameters [54, 32, 24].

- Shear two-point correlation function  $\xi_{i,j}(\theta)$  :

Another real space statistic is the shear two-point correlation function  $\xi_{i,j}(\theta)$  defined in §3, which is widely used because it is easy to implement and can be estimated even for complex geometry. The shear two-point correlation function can also be related to the underlying 3D matter power spectrum via the 2D convergence power spectrum  $P_\kappa$ . The shear two-point correlation function is the Fourier transform of the convergence power spectrum  $P_\kappa$ , which becomes a Hankel transform (also called Fourier-Bessel transform) considering the isotropy of the Universe:

$$\xi_+(\theta) = \xi_{1,1}(\theta) + \xi_{2,2}(\theta) = \int_0^\infty \frac{dl}{2\pi} l P_\kappa(l) J_0(l\theta), \quad (52)$$

where  $J_0$  corresponds to the Bessel function at zero order.

The two-point correlation function is the most popular statistical tool used in weak lensing analysis. It has been used in many recent weak lensing analyses to constrain cosmological parameters (see for example [7, 32, 24]).

The simplest way to compute a two-point correlation function consists in counting the number of background galaxy pairs separated by a distance  $d$ . But this brute force approach has a complexity of  $O(N^2)$ , which becomes an important computational load for large surveys. Recently, some progress has been made in this field, and new methods have been developed to speed up the calculation of the two-point correlation function by reducing the complexity to  $O(N \log N)$ . These algorithms are based on ordered binary trees that are an interesting data structure to scan the galaxy

pairs [96, 63]. But to reach this complexity some approximations are required, such as neglecting large scales or binning the two-point correlation function [37, 96].

- Shear Tomography  $\xi_{i,j}^{k,l}(\theta)$  :

The constraints on cosmological parameters can be significantly improved if the shape measurements are combined with photometric redshifts. The 2D shear correlation formalism can be extended to 3D shear by splitting the galaxy sample into redshift bins from which the auto- and cross-correlations can be calculated. It is the so-called cosmic shear tomography [34, 2]. The shear cross-correlation functions  $\xi_{i,j}^{k,l}(\theta)$  between the bins  $k$  and  $l$  are defined as follows:

$$\xi_{i,j}^{k,l}(\theta) = \langle \gamma_i^k(\vec{\theta}') \gamma_j^l(\vec{\theta}' + \vec{\theta}) \rangle. \quad (53)$$

The shear cross-correlation functions  $\xi_{i,j}^{k,l}(\theta)$  can be related to the underlying 3D matter power spectrum via the 2D convergence cross-power spectrum  $P_\kappa^{k,l}$  by the following relation:

$$\xi_+^{k,l}(\theta) = \int_0^\infty \frac{dl}{2\pi} l P_\kappa^{k,l}(l) J_0(l\theta), \quad (54)$$

with:

$$P_\kappa^{k,l}(l) = \frac{9}{16} \left( \frac{H_0}{c} \right)^4 \Omega_m^2 \int d\chi \frac{g^k(\chi) g^l(\chi)}{(ar(\chi))^2} P \left( \frac{l}{r}, \chi \right), \quad (55)$$

Shear tomography has been applied to real data (e.g. [4, 76]) to improve the constraints on cosmological parameters. The separation of source galaxies into tomographic bins improves significantly the constraints on cosmological parameters, and particularly those of dark energy that drives cosmic expansion.

- Second-order statistics to separate E and B modes :

If the shear, estimated from the image shapes of distant galaxies, was only due to gravitational lensing, then it should consist only of a pure E-mode shear (see §4.2). But the estimated shear may contain systematic errors. Therefore, the splitting of the observed shear field into its E- and B-modes is of great importance to isolate the gravitational shear from the shear components most likely not due to lensing. The standard technique for this separation is the variance of the aperture mass  $\langle M_{ap}^2 \rangle$  [74], which corresponds to an average shear two-point correlation. This statistic is the result of the convolution of the shear two-point correlation with a compensated filter. Several forms of filters have been suggested which trade locality in real space with locality in Fourier space. By considering the filter defined by [69] with a scale of  $\theta_s$ , the variance of the aperture mass

can be expressed as a function of the 2D convergence power spectrum as follows:

$$\langle M_{ap}^2(\theta_s) \rangle = \int \frac{dl}{2\pi} l P_\kappa(l) \frac{576 J_4^2(l\theta_s)}{(l\theta_s)^4}. \quad (56)$$

This method has been used in many weak lensing analyses to constrain cosmological parameters (see for example [94, 82, 32, 24]). However, the lack of knowledge of the shear correlation function on very small scales introduces a systematic bias on the variance aperture method. More recently, new second-order statistic, i.e. the ring statistic [72] and COSEBIs (Complete Orthogonal Sets of E-/B-mode Integrals) [71] have been proposed to overcome the practical problem encountered by the aperture mass method.

Second-order statistics measure the Gaussian properties of the field, which limits the amount of information extracted, since it is known that the low redshift Universe is highly non-Gaussian on small scales. Indeed, gravitational clustering is a non linear process and, in particular, at small scales the mass distribution is highly non-Gaussian. Consequently, if only second-order statistics are used to place constraints on the cosmological model, degenerate constraints are obtained between some important cosmological parameters (see for example [33, 24, 76]).

### 6.3 Non-Gaussian statistics

If the weak lensing signal was Gaussian, it would be fully described by its angular power spectrum. However, in the standard model of structure formation, fluctuations that are initially Gaussian are amplified by gravitational collapse to produce a highly non-Gaussian matter distribution. Thus, except at large scale, the convergence field is highly non-Gaussian. On small scales, we can observe structures like galaxies and clusters of galaxies, and on intermediate scales, we observe some filamentary structures. The characterization of this non-Gaussianity can be used to constrain the cosmological parameters. A possible solution is to consider higher-order statistics of the shear or convergence field. The statistics presented below are estimated in the convergence field because the non-Gaussianity is clearly visible in the field.

Third-order statistics are the lowest-order statistics which can be used to detect non-Gaussianity. Many authors have already addressed the problem of three-point statistics and semi-analytical predictions for the three-point correlation function and the bispectrum have already been derived (e.g. [51, 52, 78, 19]). However, the correction for missing data in the full higher-order Fourier statistics remains an outstanding issue. An alternative solution (see §4.3) has been proposed by [67] to derive second-order and third-order statistics and possibly higher-order statistics from an incomplete shear map.

- The Convergence Bispectrum  $B_\kappa(|\vec{l}_1|, |\vec{l}_2|, |\vec{l}_3|)$ :  
By analogy with second-order statistics, whatever the third-order statistic considered, it can be easily related to the convergence bispectrum  $B_\kappa(|\vec{l}_1|, |\vec{l}_2|, |\vec{l}_3|)$ , which is the Fourier analog of the three-point correlation function:

$$B_\kappa(|\vec{l}_1|, |\vec{l}_2|, |\vec{l}_3|) \propto \langle \hat{\kappa}(|\vec{l}_1|) \hat{\kappa}(|\vec{l}_2|) \hat{\kappa}^*(|\vec{l}_3|) \rangle. \quad (57)$$

where  $\kappa^*$  is the complex conjugate of  $\kappa$ . The bispectrum only depends on distances  $|\vec{l}_1|$ ,  $|\vec{l}_2|$  and  $|\vec{l}_3|$ . [77] proposed an algorithm to compute the bispectrum from numerical simulations using a Fast Fourier transform but without considering the case of incomplete data. This method is used by [23] to estimate the bispectrum from numerical simulations in order to compare it with the semi-predictions of the analytic halo model.

- Convergence three-point correlation function  $\xi_{i,j,k}(\theta)$ :  
The three-point correlation function  $\xi_{i,j,k}$  is easy to estimate and can be estimated even for complex geometry. It is defined as follows :

$$\xi_{i,j,k}(\theta) = \langle \kappa(\vec{\theta}_1) \kappa(\vec{\theta}_2) \kappa(\vec{\theta}_3) \rangle. \quad (58)$$

The same relation can be derived for the shear. It has been shown that tighter constraints can be obtained with the three-point correlation function [87]. Estimating three-point correlation function from data has already been done [9] but can not be considered in future large data sets because it is computationally too intensive. In the conclusion of [86], the authors briefly suggested to use the  $p$ -point correlation functions with implementations that are at best  $O(N(\log N)^{p-1})$ . However, it was not clear if this suggestion is valid for the missing data case.

- Third-order moment of the convergence  $S_\kappa$ :  
A simpler quantity than the three-point correlation function is provided by measuring the third-order moment of the convergence  $\kappa$ , also named the skewness, that measures the asymmetry of the distribution [66]:

$$S_\kappa = \sum_{i=1}^N \frac{(\kappa_i - \bar{\kappa})^3}{(N-1)\sigma^3}. \quad (59)$$

The convergence skewness is primarily due to rare and massive dark matter halos. The distribution will be more or less skewed positively depending on the abundance of rare and massive halos.

- Fourth-order moment of the convergence  $K_\kappa$ :  
We can also estimate the fourth-order moment of the convergence, also known as kurtosis, that measures the peakiness of a distribution [66]: The

kurtosis of the convergence  $\kappa$  is defined as follows :

$$K_\kappa = \sum_{i=1}^N \frac{(\kappa_i - \bar{\kappa})^4}{(N-1)\sigma^4} - 3, \quad (60)$$

which is known as excess kurtosis. A high kurtosis distribution has a sharper “peak” and flatter “tails”, while a low kurtosis distribution has a more rounded peak.

- The skewness and the kurtosis of the aperture mass  $\langle M_{ap}^n \rangle$ :  
Similarly to the aperture mass variance described in the previous section, the skewness and the kurtosis of the aperture mass have also been introduced to weak lensing analyses to constrain cosmological parameters (see for example [38, 73]).
- Peak Counting (PC)  
As said previously, the convergence field is highly non-Gaussian. Another approach to look for non-Gaussianity is to perform a statistical analysis directly on the non-Gaussian structures present in the convergence field. For example, galaxy clusters, which are the largest virialized cosmological structures in the Universe, can provide a unique way to focus on non-Gaussianity present at small scales. One interesting method is the Peak Counting, which searches the number of peaks detected on the field that differs from the cluster abundance because of the projection of the large scale structures. The peak counting has been used to measure the number of peaks detected on the convergence field by [36, 26, 48]. Peaks can be also counted on the shear field using a filtered version of the shear [20].

It has been proposed by [66] to do a comparison between several statistics and several representations. The comparison shows that the wavelet transform makes statistics more sensitive to the non-Gaussianity present in the convergence field. In the same paper, several non-Gaussian statistics have been compared and the peak counting estimated in a wavelet representation, called Wavelet Peak Counting, has been found to be the best non-Gaussian statistic to constrain cosmological parameters. In this paper, the comparison with bispectrum was restricted to the equilateral configuration. In [8], the authors shows that bispectrum using all triangle configurations outperforms peak counting as a function of clusters’ mass and redshift.

## 7 Conclusion

The weak gravitational lensing effect, which is directly sensitive to the gravitational potential, provides a unique method to map the 3D dark matter distribution and thus understand the process of structure formation. This can be used to set tighter constraints on cosmological models and to better understand the

nature of dark matter and dark energy. But the constraints derived from this weak lensing effect depend on the techniques used to analyze the weak lensing signal, which is very weak.

The field of weak gravitational lensing has recently seen great success in mapping the distribution of dark matter (Fig. 8). The next breakthrough will certainly happen in the next decade thanks to the future full-sky missions designed to weak gravitational lensing: ground-based missions like LSST (Large Synoptic Survey Telescope) or space-based missions like Euclid or WFIRST (Wide Field Infrared Survey Telescope). The primary goal of these missions is precisely to map very accurately the geometry of the dark universe and its evolution by measuring shapes and redshifts of galaxies over the entire sky. It will provide a 3D full-sky map of the dark and visible matter in the Universe and will permit to set tighter constraints on Dark Energy and other cosmological parameters. For this to happen, new methods are now necessary to reach the accuracy required by this survey, and ongoing efforts are needed to improve the standard analyses. This chapter attempts to give an overview of the techniques that are currently used to analyze the weak lensing signal along with future directions. It shows that weak lensing is a dynamic research area in constant progress.

In this chapter, we have detailed the different steps of the weak lensing data analysis, thus presenting various aspects of signal processing. For each problem, we have systematically presented a range of methods currently used, from earliest to up-to-date methods. This chapter highlights the introduction of Bayesian ideas that have provided a way to incorporate prior knowledge in data analysis as a major milestone in weak lensing analysis. The next major step might possibly be the introduction of sparsity. Indeed, we have presented new methods based on sparse representations of the data that have already had some success.

## Acknowledgements

This work has been supported by the European Research Council grant SparseAstro (ERC-228261).

## References

- [1] A. Albrecht, G. Bernstein, R. Cahn, W. L. Freedman, J. Hewitt, W. Hu, J. Huth, M. Kamionkowski, E. W. Kolb, L. Knox, J. C. Mather, S. Staggs, and N. B. Suntzeff. Report of the Dark Energy Task Force. *ArXiv Astrophysics e-prints : astro-ph/0609591*, September 2006.
- [2] A. Amara and A. Réfrégier. Optimal surveys for weak-lensing tomography. *MNRAS*, 381:1018–1026, November 2007.
- [3] D. J. Bacon and A. N. Taylor. Mapping the 3D dark matter potential with weak shear. *MNRAS*, 344:1307–1326, October 2003.
- [4] D. J. Bacon, A. N. Taylor, M. L. Brown, M. E. Gray, C. Wolf, K. Meisenheimer, S. Dye, L. Wisotzki, A. Borch, and M. Kleinheinrich. Evolution of the dark matter distribution with three-dimensional weak lensing. *MNRAS*, 363:723–733, November 2005.
- [5] M. Bartelmann, R. Narayan, S. Seitz, and P. Schneider. Maximum-likelihood Cluster Reconstruction. *ApJ*, 464:L115+, June 1996.
- [6] M. Bartelmann and P. Schneider. Weak gravitational lensing. *Phys. Rep.*, 340:291–472, January 2001.
- [7] J. Benjamin, C. Heymans, E. Semboloni, L. van Waerbeke, H. Hoekstra, T. Erben, M. D. Gladders, M. Hetterscheidt, Y. Mellier, and H. K. C. Yee. Cosmological constraints from the 100 deg<sup>2</sup> weak-lensing survey. *MNRAS*, 381:702–712, October 2007.
- [8] J. Bergé, A. Amara, and A. Réfrégier. Optimal Capture of Non-Gaussianity in Weak-Lensing Surveys: Power Spectrum, Bispectrum, and Halo Counts. *ApJ*, 712:992–1002, April 2010.
- [9] F. Bernardeau, Y. Mellier, and L. van Waerbeke. Detection of non-Gaussian signatures in the VIRMOS-DESCART lensing survey. *A&A*, 389:L28–L32, July 2002.
- [10] G. M. Bernstein. Comprehensive Two-Point Analyses of Weak Gravitational Lensing Surveys. *ApJ*, 695:652–665, April 2009.
- [11] G. M. Bernstein and M. Jarvis. Shapes and Shears, Stars and Smears: Optimal Measurements for Weak Lensing. *AJ*, 123:583–618, February 2002.
- [12] G. M. Bernstein and M. Jarvis. Shapes and Shears, Stars and Smears: Optimal Measurements for Weak Lensing. *AJ*, 123:583–618, February 2002.
- [13] S. Bridle and L. King. Dark energy constraints from cosmic shear power spectra: impact of intrinsic alignments on photometric redshift requirements. *New Journal of Physics*, 9:444–+, December 2007.

- [14] S. Bridle, J.-P. Kneib, S. Bardeau, and S. Gull. Bayesian galaxy shape estimation. In P. Natarajan, editor, *The Shapes of Galaxies and their Dark*, pages 38–+, 2002.
- [15] S. Bridle, J. Shawe-Taylor, A. Amara, D. Applegate, S. T. Balan, G. Bernstein, J. Berge, H. Dahle, T. Erben, M. Gill, A. Heavens, C. Heymans, F. W. High, H. Hoekstra, M. Jarvis, D. Kirk, T. Kitching, J.-P. Kneib, K. Kuijken, D. Lagatutta, R. Mandelbaum, R. Massey, Y. Mellier, B. Moghaddam, Y. Moudén, R. Nakajima, S. Paulin-Henriksson, S. Pires, A. Rasat, A. Refregier, J. Rhodes, T. Schrabback, E. Semboloni, M. Shmakova, L. van Waerbeke, D. Witherick, L. Voigt, and D. Wittman. Handbook for the GREAT08 Challenge: An image analysis competition for cosmological lensing. *Annals of Applied Statistics*, 3:6–37, 2009.
- [16] S. L. Bridle, M. P. Hobson, A. N. Lasenby, and R. Saunders. A maximum-entropy method for reconstructing the projected mass distribution of gravitational lenses. *MNRAS*, 299:895–903, September 1998.
- [17] E. Candès, L. Demanet, D. Donoho, and Y. Lexing. Fast Discrete Curvelet Transforms. *SIAM. Multiscale Model. Simul.*, 5.:861–899, 2006.
- [18] E. Candès and D. Donoho. ridgelets: a key to higher dimensional intermittency. *Philosophical Transactions of the Royal Society A*, 357:2495–2509, 1999.
- [19] A. Cooray and W. Hu. Weak Gravitational Lensing Bispectrum. *ApJ*, 548:7–18, February 2001.
- [20] J. P. Dietrich and J. Hartlap. Cosmology with the shear-peak statistics. *MNRAS*, 402:1049–1058, February 2010.
- [21] D.L. Donoho and X. Huo. Uncertainty principles and ideal atomic decomposition. *Transactions on Information Theory*, 47:2845–2862, 2001.
- [22] M. Elad, J.-L. Starck, P. Querre, and D.L. Donoho. Simultaneous Cartoon and Texture Image Inpainting using Morphological Component Analysis (MCA). *J. on Applied and Computational Harmonic Analysis*, 19(3):340–358, 2005.
- [23] P. Fosalba, J. Pan, and I. Szapudi. Cosmological Three-Point Function: Testing the Halo Model against Simulations. *ApJ*, 632:29–48, October 2005.
- [24] L. Fu, E. Semboloni, H. Hoekstra, M. Kilbinger, L. van Waerbeke, I. Tereno, Y. Mellier, C. Heymans, J. Coupon, K. Benabed, J. Benjamin, E. Bertin, O. Doré, M. J. Hudson, O. Ilbert, R. Maoli, C. Marmo, H. J. McCracken, and B. Ménard. Very weak lensing in the CFHTLS wide: cosmology from cosmic shear in the linear regime. *A&A*, 479:9–25, February 2008.
- [25] S.-F. Gull. *Developments in maximum entropy data analysis*, volume 344. September 2003.

- [26] T. Hamana, M. Takada, and N. Yoshida. Searching for massive clusters in weak lensing surveys. *MNRAS*, 350:893–913, May 2004.
- [27] A. Heavens. 3D weak lensing. *MNRAS*, 343:1327–1334, August 2003.
- [28] C. Heymans and A. Heavens. Weak gravitational lensing: reducing the contamination by intrinsic alignments. *MNRAS*, 339:711–720, March 2003.
- [29] C. Heymans, L. Van Waerbeke, D. Bacon, J. Berge, G. Bernstein, E. Bertin, S. Bridle, M. L. Brown, D. Clowe, H. Dahle, T. Erben, M. Gray, M. Hettterscheidt, H. Hoekstra, P. Hudelot, M. Jarvis, K. Kuijken, V. Margoniner, R. Massey, Y. Mellier, R. Nakajima, A. Refregier, J. Rhodes, T. Schrabback, and D. Wittman. The Shear Testing Programme - I. Weak lensing analysis of simulated ground-based observations. *MNRAS*, 368:1323–1339, May 2006.
- [30] C. Hikage, M. Takada, T. Hamana, and D. Spergel. Shear Power Spectrum Reconstruction using Pseudo-Spectrum Method. *ArXiv e-prints*, April 2010.
- [31] H. Hoekstra, M. Franx, K. Kuijken, and G. Squires. Weak Lensing Analysis of CL 1358+62 Using Hubble Space Telescope Observations. *ApJ*, 504:636–+, September 1998.
- [32] H. Hoekstra, Y. Mellier, L. van Waerbeke, E. Semboloni, L. Fu, M. J. Hudson, L. C. Parker, I. Tereno, and K. Benabed. First Cosmic Shear Results from the Canada-France-Hawaii Telescope Wide Synoptic Legacy Survey. *ApJ*, 647:116–127, August 2006.
- [33] H. Hoekstra, H. K. C. Yee, and M. D. Gladders. Constraints on  $\Omega_m$  and  $\sigma_8$  from Weak Lensing in Red-Sequence Cluster Survey Fields. *ApJ*, 577:595–603, October 2002.
- [34] W. Hu. Power Spectrum Tomography with Weak Lensing. *ApJ*, 522:L21–L24, September 1999.
- [35] W. Hu and C. R. Keeton. Three-dimensional mapping of dark matter. *Phys. Rev. D*, 66(6):063506–+, September 2002.
- [36] B. Jain and L. Van Waerbeke. Statistics of Dark Matter Halos from Gravitational Lensing. *ApJ*, 530:L1–L4, February 2000.
- [37] M. Jarvis, G. Bernstein, and B. Jain. The skewness of the aperture mass statistic. *MNRAS*, 352:338–352, July 2004.
- [38] M. Jarvis, G. Bernstein, and B. Jain. The skewness of the aperture mass statistic. *MNRAS*, 352:338–352, July 2004.
- [39] B. Joachimi and S. L. Bridle. Simultaneous measurement of cosmology and intrinsic alignments using joint cosmic shear and galaxy number density correlations. *A&A*, 523:A1+, November 2010.

- [40] B. Joachimi and P. Schneider. The removal of shear-ellipticity correlations from the cosmic shear signal via nulling techniques. *A&A*, 488:829–843, September 2008.
- [41] B. Joachimi and P. Schneider. The removal of shear-ellipticity correlations from the cosmic shear signal. Influence of photometric redshift errors on the nulling technique. *A&A*, 507:105–129, November 2009.
- [42] N. Kaiser. Nonlinear cluster lens reconstruction. *ApJ*, 439:L1–L3, January 1995.
- [43] N. Kaiser and G. Squires. Mapping the dark matter with weak gravitational lensing. *ApJ*, 404:441–450, February 1993.
- [44] N. Kaiser, G. Wilson, and G.A. Luppino. Large-Scale Cosmic Shear Measurements. *Astrophysical Journal*, pages 318–625, 2000.
- [45] L. King and P. Schneider. Suppressing the contribution of intrinsic galaxy alignments to the shear two-point correlation function. *A&A*, 396:411–418, December 2002.
- [46] L. J. King and P. Schneider. Separating cosmic shear from intrinsic galaxy alignments: Correlation function tomography. *A&A*, 398:23–30, January 2003.
- [47] T. D. Kitching, L. Miller, C. E. Heymans, L. van Waerbeke, and A. F. Heavens. Bayesian galaxy shape measurement for weak lensing surveys - II. Application to simulations. *MNRAS*, 390:149–167, October 2008.
- [48] J. M. Kratochvil, Z. Haiman, and M. May. Probing cosmology with weak lensing peak counts. *Phys. Rev. D*, 81(4):043519–+, February 2010.
- [49] K. Kuijken. Shears from shapelets. *A&A*, 456:827–838, September 2006.
- [50] G. A. Luppino and N. Kaiser. Detection of Weak Lensing by a Cluster of Galaxies at  $Z = 0.83$ . *ApJ*, 475:20–+, January 1997.
- [51] C.-P. Ma and J. N. Fry. Deriving the Nonlinear Cosmological Power Spectrum and Bispectrum from Analytic Dark Matter Halo Profiles and Mass Functions. *ApJ*, 543:503–513, November 2000.
- [52] C.-P. Ma and J. N. Fry. What Does It Take to Stabilize Gravitational Clustering? *ApJ*, 538:L107–L111, August 2000.
- [53] S. Mallat. A theory for Multiresolution Signal Decomposition the wavelet Representation. *IPAMI*, 11:674–693, 1989.
- [54] R. Maoli, L. Van Waerbeke, Y. Mellier, P. Schneider, B. Jain, F. Bernardeau, T. Erben, and B. Fort. Cosmic shear analysis in 50 uncorrelated VLT fields. Implications for  $\Omega_0$ ,  $\sigma_8$ . *A&A*, 368:766–775, March 2001.

- [55] P. J. Marshall, M. P. Hobson, S. F. Gull, and S. L. Bridle. Maximum-entropy weak lens reconstruction: improved methods and application to data. *MNRAS*, 335:1037–1048, October 2002.
- [56] R. Massey, C. Heymans, J. Bergé, G. Bernstein, S. Bridle, D. Clowe, H. Dahle, R. Ellis, T. Erben, M. Hettterscheidt, F. W. High, C. Hirata, H. Hoekstra, P. Hudelot, M. Jarvis, D. Johnston, K. Kuijken, V. Margoniner, R. Mandelbaum, Y. Mellier, R. Nakaajima, S. Paulin-Henriksson, M. Peebles, C. Roat, A. Refregier, J. Rhodes, T. Schrabback, M. Schirmer, U. Seljak, E. Semboloni, and L. van Waerbeke. The Shear Testing Programme 2: Factors affecting high-precision weak-lensing analyses. *MNRAS*, 376:13–38, March 2007.
- [57] R. Massey and A. Refregier. Polar shapelets. *MNRAS*, 363:197–210, October 2005.
- [58] R. Massey, A. Refregier, D. J. Bacon, R. Ellis, and M. L. Brown. An enlarged cosmic shear survey with the William Herschel Telescope. *MNRAS*, 359:1277–1286, June 2005.
- [59] R. Massey, J. Rhodes, R. Ellis, N. Scoville, A. Leauthaud, A. Finoguenov, P. Capak, D. Bacon, H. Aussel, J.-P. Kneib, A. Koekemoer, H. McCracken, B. Mobasher, S. Pires, A. Refregier, S. Sasaki, J.-L. Starck, Y. Taniguchi, A. Taylor, and J. Taylor. Dark matter maps reveal cosmic scaffolding. *Nature*, 445:286–290, January 2007.
- [60] R. Massey, J. Rhodes, A. Leauthaud, P. Capak, R. Ellis, A. Koekemoer, A. Réfrégier, N. Scoville, J. E. Taylor, J. Albert, J. Bergé, C. Heymans, D. Johnston, J.-P. Kneib, Y. Mellier, B. Mobasher, E. Semboloni, P. Shopbell, L. Tasca, and L. Van Waerbeke. COSMOS: Three-dimensional Weak Lensing and the Growth of Structure. *ApJS*, 172:239–253, September 2007.
- [61] Y. Mellier. Probing the Universe with Weak Lensing. *Annual Review of Astronomy and Astrophysics*, 37:127–189, 1999.
- [62] L. Miller, T. D. Kitching, C. Heymans, A. F. Heavens, and L. van Waerbeke. Bayesian galaxy shape measurement for weak lensing surveys - I. Methodology and a fast-fitting algorithm. *MNRAS*, 382:315–324, November 2007.
- [63] A. W. Moore, A. J. Connolly, C. Genovese, A. Gray, L. Grone, N. I. Kanidoris, R. C. Nichol, J. Schneider, A. S. Szalay, I. Szapudi, and L. Wasserman. Fast Algorithms and Efficient Statistics: N-Point Correlation Functions. In A. J. Banday, S. Zaroubi, and M. Bartelmann, editors, *Mining the Sky*, pages 71–+, 2001.
- [64] D. Munshi, P. Valageas, L. van Waerbeke, and A. Heavens. Cosmology with weak lensing surveys. *Phys. Rep.*, 462:67–121, June 2008.

- [65] E. Pantin and J.-L. Starck. Deconvolution of astronomical images using the multiscale maximum entropy method. *A&AS*, 118:575–585, September 1996.
- [66] S. Pires, J.-L. Starck, A. Amara, A. Réfrégier, and R. Teyssier. Cosmological model discrimination with weak lensing. *A&A*, 505:969–979, October 2009.
- [67] S. Pires, J.-L. Starck, A. Amara, R. Teyssier, A. Réfrégier, and J. Fadili. FAst STatistics for weak Lensing (FASTLens): fast method for weak lensing statistics and map making. *MNRAS*, 395:1265–1279, May 2009.
- [68] A. Refregier. Weak Gravitational Lensing by Large-Scale Structure. *ARA&A*, 41:645–668, 2003.
- [69] P. Schneider. Detection of (dark) matter concentrations via weak gravitational lensing. *MNRAS*, 283:837–853, December 1996.
- [70] P. Schneider. *Proceeding of the 33rd Saas-Fee Advanced Course*, chapter Weak Gravitational Lensing. 2003.
- [71] P. Schneider, T. Eifler, and E. Krause. COSEBIs: Extracting the full E-/B-mode information from cosmic shear correlation functions. *A&A*, 520:A116+, September 2010.
- [72] P. Schneider and M. Kilbinger. The ring statistics - how to separate E- and B-modes of cosmic shear correlation functions on a finite interval. *A&A*, 462:841–849, February 2007.
- [73] P. Schneider, M. Kilbinger, and M. Lombardi. The three-point correlation function of cosmic shear. II. Relation to the bispectrum of the projected mass density and generalized third-order aperture measures. *A&A*, 431:9–25, February 2005.
- [74] P. Schneider, L. van Waerbeke, B. Jain, and G. Kruse. A new measure for cosmic shear. *MNRAS*, 296:873–892, June 1998.
- [75] T. Schrabback, J. Hartlap, B. Joachimi, M. Kilbinger, P. Simon, K. Benabed, M. Bradač, T. Eifler, T. Erben, C. D. Fassnacht, F. W. High, S. Hilbert, H. Hildebrandt, H. Hoekstra, K. Kuijken, P. J. Marshall, Y. Mellier, E. Morganson, P. Schneider, E. Semboloni, L. van Waerbeke, and M. Velander. Evidence of the accelerated expansion of the Universe from weak lensing tomography with COSMOS. *A&A*, 516:A63+, June 2010.
- [76] T. Schrabback, J. Hartlap, B. Joachimi, M. Kilbinger, P. Simon, K. Benabed, M. Bradač, T. Eifler, T. Erben, C. D. Fassnacht, F. W. High, S. Hilbert, H. Hildebrandt, H. Hoekstra, K. Kuijken, P. J. Marshall, Y. Mellier, E. Morganson, P. Schneider, E. Semboloni, L. van Waerbeke, and M. Velander. Evidence of the accelerated expansion of the Universe from weak lensing tomography with COSMOS. *A&A*, 516:A63+, June 2010.

- [77] R. Scoccimarro, S. Colombi, J. N. Fry, J. A. Frieman, E. Hivon, and A. Melott. Nonlinear Evolution of the Bispectrum of Cosmological Perturbations. *ApJ*, 496:586–+, March 1998.
- [78] R. Scoccimarro and H. M. P. Couchman. A fitting formula for the nonlinear evolution of the bispectrum. *MNRAS*, 325:1312–1316, August 2001.
- [79] S. Seitz and P. Schneider. Cluster lens reconstruction using only observed local data: an improved finite-field inversion technique. *A&A*, 305:383–+, January 1996.
- [80] S. Seitz, P. Schneider, and M. Bartelmann. Entropy-regularized maximum-likelihood cluster mass reconstruction. *A&A*, 337:325–337, September 1998.
- [81] U. Seljak. Weak Lensing Reconstruction and Power Spectrum Estimation: Minimum Variance Methods. *ApJ*, 506:64–79, October 1998.
- [82] E. Semboloni, Y. Mellier, L. van Waerbeke, H. Hoekstra, I. Tereno, K. Benabed, S. D. J. Gwyn, L. Fu, M. J. Hudson, R. Maoli, and L. C. Parker. Cosmic shear analysis with CFHTLS deep data. *A&A*, 452:51–61, June 2006.
- [83] P. Simon, A. N. Taylor, and J. Hartlap. Unfolding the matter distribution using three-dimensional weak gravitational lensing. *MNRAS*, 399:48–68, October 2009.
- [84] J. L. Starck, D. L. Donoho, and E. J. Candès. Astronomical image representation by the curvelet transform. *A&A*, 398:785–800, February 2003.
- [85] J.-L. Starck, S. Pires, and A. Réfrégier. Weak lensing mass reconstruction using wavelets. *A&A*, 451:1139–1150, June 2006.
- [86] I. Szapudi, S. Prunet, D. Pogosyan, A. S. Szalay, and J. R. Bond. Fast Cosmic Microwave Background Analyses via Correlation Functions. *ApJ*, 548:L115–L118, February 2001.
- [87] M. Takada and B. Jain. Three-point correlations in weak lensing surveys: model predictions and applications. *MNRAS*, 344:857–886, September 2003.
- [88] M. Takada and M. White. Tomography of Lensing Cross-Power Spectra. *ApJ*, 601:L1–L4, January 2004.
- [89] A. Taylor. New Dimensions in Cosmic Lensing. In *The Davis Meeting On Cosmic Inflation*, March 2003.
- [90] A. N. Taylor. Imaging the 3-D cosmological mass distribution with weak gravitational lensing. *ArXiv Astrophysics e-prints : astro-ph/0111605*.

- [91] A. N. Taylor, D. J. Bacon, M. E. Gray, C. Wolf, K. Meisenheimer, S. Dye, A. Borch, M. Kleinheinrich, Z. Kovacs, and L. Wisotzki. Mapping the 3D dark matter with weak lensing in COMBO-17. *MNRAS*, 353:1176–1196, October 2004.
- [92] R. Teyssier, S. Pires, S. Prunet, D. Aubert, C. Pichon, A. Amara, K. Benabed, S. Colombi, A. Refregier, and J.-L. Starck. Full-sky weak-lensing simulation with 70 billion particles. *A&A*, 497:335–341, April 2009.
- [93] C. Vale and M. White. Simulating Weak Lensing by Large-Scale Structure. *ApJ*, 592:699–709, August 2003.
- [94] L. Van Waerbeke, Y. Mellier, R. Pelló, U.-L. Pen, H. J. McCracken, and B. Jain. Likelihood analysis of cosmic shear on simulated and VIRMOS-DESCART data. *A&A*, 393:369–379, October 2002.
- [95] J. T. VanderPlas, A. J. Connolly, B. Jain, and M. Jarvis. Three-dimensional Reconstruction of the Density Field: An SVD Approach to Weak-lensing Tomography. *ApJ*, 727:118–+, February 2011.
- [96] L. L. Zhang and U.-L. Pen. Fast n-point correlation functions and three-point lensing application. *nature*, 10:569–590, July 2005.